Momentum Dependence of the Superconducting Gap in $Bi_2Sr_2CaCu_2O_8$

H. Ding,[1,2] J. C. Campuzano,[1,2] A. F. Bellman,[1,5] T. Yokoya,[3] M. R. Norman,[1] M. Randeria,[1] T. Takahashi,[3] H. Katayama-Yoshida,[3] T. Mochiku,[4] K. Kadowaki,[4] and G. Jennings[1]

[1]*Materials Science Division, Argonne National Laboratory, Argonne, Illinois 60439*
[2]*Department of Physics, University of Illinois at Chicago, Chicago, Illinois 60607*
[3]*Department of Physics, Tohoku University, Sendai 980, Japan*
[4]*National Research Institute for Metals, Sengen, Tsukuba, 305 Ibaraki, Japan*
[5]*Dipartimento di Fisica, Università di Milano, 20133 Milano, Italy*

(Received 20 October 1994)

We measure the momentm dependence of the superconducting gap along the Fermi surface of $Bi_2Sr_2CaCu_2O_8$ by high resolution angle-resolved photoemission spectroscopy. The gap is large in the vicinity of the $\overline{M}$ point (where Γ-$\overline{M}$ is along the Cu-O bond), and small along the Γ-X and Γ-Y (π, π) directions. However, the gap is not zero along these directions, but, within our accuracy, becomes zero about 10° on either side of the (π, π) directions. We discuss the implications of these results for the symmetry of the order parameter.

PACS numbers: 74.25.Jb, 71.25.Hc, 74.72.Hs, 79.60.Bm

Over the past few years, there has been a lively debate in the literature [1] concerning the nature of the superconducting order parameter in the cuprate high temperature superconductors. Low temperature penetration depth measurements on $YBa_2Cu_3O_{6.95}$ indicate the existence of line nodes in the energy gap [2]. There is an important open question whether the position of these nodes is determined by symmetry, as in the d-wave scenario, or not, as in the anisotropic s-wave scenario. Using high energy resolution angle-resolved photoemission spectroscopy (ARPES) on $Bi_2Sr_2CaCu_2O_8$ (Bi2212) [3], we determine the full momentum dependence of the gap in the two irreducible quadrants of the Brillouin zone (BZ), and we see significant anisotropy as in previous work [4,5]. We find that this momentum dependence is nontrivial, with the energy gap exhibiting two nodes on either side of the (π, π) directions in contrast to the d-wave interpretation of Ref. [4]. The simplest interpretation favors anisotropic s-wave pairing; however, possible complications are discussed below.

The results presented here depend crucially on samples of very high quality and the high energy resolution of the spectrometer, obtained by using a commercial spectrometer, but with improved electronics and shielding. The measurements were carried out at the Synchrotron Radiation Center, Wisconsin, using a high resolution 4-m normal incidence monochromator with a resolving power of 10^4 at 10^{11} photons/s. The crystals are grown by the traveling solvent floating zone method using an infrared mirror furnace. Typical samples have superconducting transitions at 87 K and widths of 1 K, as determined by a SQUID magnetometer. These single crystals have very low defect densities, as evidenced by the sharp peaks in the rocking curves in high resolution x-ray diffraction, which yield a large structural coherence length of ~1250 Å. Most importantly, from the point of view of ARPES measurements, these crystals have very flat surfaces after cleaving, as measured by specular laser reflections, with no detectable degradation of the laser's divergence. These properties reflect themselves in the ARPES energy distribution curves (EDC's) as very sharp quasiparticle peaks with extremely low background and substantial dispersion, which in turn allows an accurate determination of the Fermi surface (FS) and superconducting energy gap.

In Fig. 1(a) we show three normal-state EDC's obtained at 95 K, at momentum intervals of $\frac{1}{32}$th of the BZ dimension along the Γ-Y symmetry line ($\overline{\Gamma Y}$), with the middle curve corresponding to $\mathbf{k} = \mathbf{k}_F$. This large dispersion requires high alignment accuracy: The specimens are carefully oriented in the sample holder to an accuracy of 1° by Laue diffraction. The orientation is further confirmed via the observed symmetry of sharp photoemission features around high symmetry points. The crystals were cleaved and measured in a vacuum of $<5 \times 10^{-11}$ Torr. This is significant because residual gas adsorption affects the measured values of the gap. We did not detect any changes in the time it took to complete a set of spectra.

Figure 1(b) shows the FS obtained from normal-state measurements at 95 K (open circles) [6]. The thick line is the FS corresponding to a tight-binding fit [7] to the dispersion data (not shown here) in the ΓY quadrant. The thin lines are $\pm\mathbf{q}$ umklapps of the fundamental surface, where $\mathbf{q}$ is the Bi2212 superlattice vector $(0.21\pi, 0.21\pi)$ [8]. These umklapp sheets show remarkable agreement with other experimental FS crossings observed in the ΓY quadrant. We suggest that this is the origin of some of the features attributed to magnetic scattering in earlier work [9]. Note that only one fundamental FS is seen, implying that the interlayer coupling is too weak to resolve the two Cu-O bands.

Figure 2 shows the experimental spectra obtained at 13 K at points on the FS labeled 1 through 17, shown as filled circles in the rightmost panels. In each panel we plot one energy distribution curve (EDC) of Bi2212, and one spectrum from Pt [10] which is in electrical

 0031-9007/95/74(14)/2784(4)$06.00

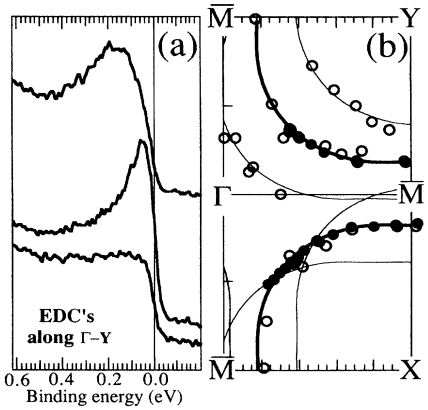

FIG. 1. (a) EDC's along the ΓY direction, showing three curves, for $\mathbf{k} < \mathbf{k}_F$ (top curve), $\mathbf{k} = \mathbf{k}_F$ (middle curve), and $\mathbf{k} > \mathbf{k}_F$ (bottom curve). k separation is $\frac{1}{32}$th of the BZ dimension; (b) FS obtained from normal-state measurements (open circles) and measurement points in the superconducting state (filled circles). The thick line is the FS obtained by a tight-binding fit to the dispersion data. The thin lines are $(0.21\pi,0.21\pi)$ umklapps of the main FS.

contact with the sample is measured at a similar angle to ensure an accurate value of E_F. The Bi2212 spectra were carefully chosen from a much more extensive set using the criterion that the leading edge of each spectrum has the largest slope among the neighboring ones, or, equivalently, the energy shift away from E_F has a local minimum. We emphasize that this criterion [results denoted by filled circles in Fig. 1(b)] yields the same location in momentum space as the normal-state FS (open circles), so that $\mathbf{k} = \mathbf{k}_F$.

We now describe our procedure for data analysis. Because of the lack of any significant 3D dispersion in Bi2212, for a c-axis oriented crystal, the ARPES intensity is proportional to $f(\omega)A(\mathbf{k},\omega)$, where $f(\omega)$ is the Fermi function, and $A(\mathbf{k},\omega)$ is the one-particle spectral function (assuming the validity of the sudden approximation and neglecting shake-off processes). We use a phenomenologically broadened BCS spectral function [11] $A(\mathbf{k},\omega) = u_{\mathbf{k}}^2\Gamma/\pi[(\omega - E_{\mathbf{k}})^2 + \Gamma^2] + v_{\mathbf{k}}^2\Gamma/\pi[(\omega + E_{\mathbf{k}})^2 + \Gamma^2]$, where the coherence factors are $v_{\mathbf{k}}^2 = 1 - u_{\mathbf{k}}^2 = \frac{1}{2}(1 - \varepsilon_{\mathbf{k}}/E_{\mathbf{k}})$. The normal-state energy ε_k is measured from E_F and the Bogoliubov quasiparticle energy is $E_{\mathbf{k}} = \sqrt{\varepsilon_{\mathbf{k}}^2 + |\Delta_{\mathbf{k}}|^2}$, where $\Delta_{\mathbf{k}}$ is the gap function. For simplicity, in the range of small ω of interest here, we choose a linewidth Γ independent of $\mathbf{k}$ and ω. Note that for $\varepsilon_{\mathbf{k}} = 0$, or $\mathbf{k} = \mathbf{k}_F$, the peak in the ARPES intensity is located at the gap, $E_{\mathbf{k}} = |\Delta_{\mathbf{k}}|$. If $\varepsilon_k \neq 0$, then the shift of the measured peak will be larger than the actual gap, since the peak of the spectral function will be at $E_{\mathbf{k}} \geq |\Delta_{\mathbf{k}}|$. To avoid overestimating the gap, we search in momentum space for the *minimum measurable gap,* as explained above.

The EDC is given by

$$I(\mathbf{k},\omega) = I_0 \int_{\delta\mathbf{k}} d\mathbf{k}' \int d\omega' R(\omega - \omega') f(\omega') A(\mathbf{k}',\omega'),$$

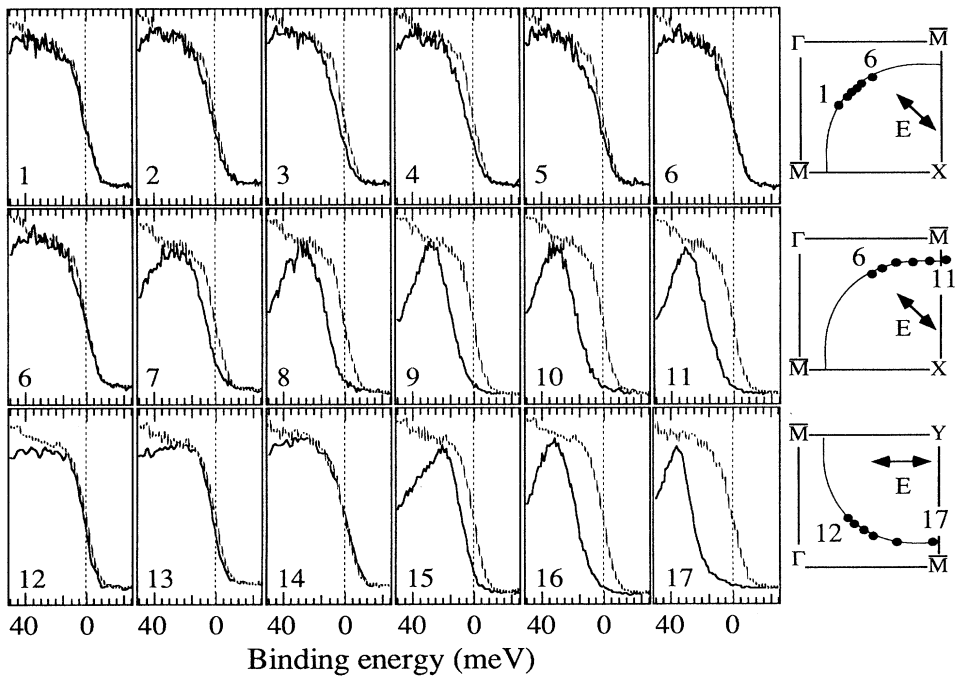

FIG. 2. EDC's of Bi2212 (solid lines) in the vicinity of E_F, at values of momenta corresponding to the numbered points in the rightmost panels. The panels on the right also indicate the polarization of the photons. The EDC of Pt (broken line) used as a reference is also shown for each measurement.

where the overall intensity I_0 represents matrix elements and normalization, the momentum integration is over an interval $\delta\mathbf{k}$ given by the window of the analyzer ($\pm 1°$), and the energy resolution function $R(\omega)$ is a Gaussian of standard deviation of 8 meV (FWHM of 18.8 meV). In addition, we add a background [12] which improves the fit at large binding energies, but has no effect on the gap estimate.

In Fig. 3 we show the results of EDC's calculated using the above formulas, together with the ARPES data at selected points along the FS. In effect, only two parameters, the gap $\Delta_\mathbf{k}$ and the overall intensity I_0, are varied for each curve. The linewidth Γ plays no role in the quality of the fits to the leading edge at 13 K, and the trailing edge is always broadened by the background. We expect that a more realistic $\Gamma(\mathbf{k}, \omega)$ would account for some of the broadening of the trailing edge being attributed here to the background in the fits.

First consider the spectrum near the $\overline{M}$ point (labeled 17). From detailed temperature dependent studies, which will be published elsewhere, we find that the observed linewidth decreases dramatically with the lowering of T below T_c [13]. At 13 K, Γ has become so small that the width of the experimental spectrum is dominated by the energy resolution. In fact, all of our fits to the leading edge are insensitive to the precise value of Γ, and we use

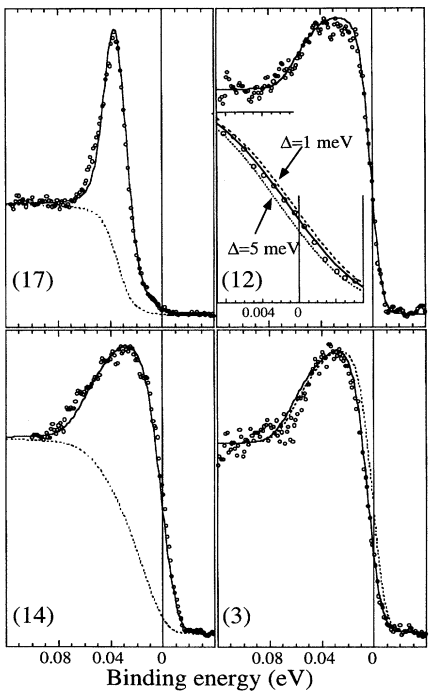

FIG. 3. Selected fits of data points in Fig. 2 (same labels), using the formulas in the text. Top left: near $\overline{M}$; top right: along ΓY, and the inset shows an expanded view near E_F; bottom left: at the node in the ΓY quadrant; bottom right: along ΓX. Backgrounds are shown for spectra 14 and 17 as dashed lines, and a zero gap curve is shown for spectrum 3.

the same value of 3.5 meV, independent of the location on the FS. Furthermore, the momentum window $\delta\mathbf{k}$ of $\pm 1°$ does not affect the spectrum near the $\overline{M}$ point since the band has a very flat dispersion. Assuming that $\varepsilon_\mathbf{k} = 0$, the only parameters to which the fit is sensitive are $\Delta_\mathbf{k}$ and I_0. Based on the overall quality of this fit, we find $|\Delta_\mathbf{k}| = 34 \pm 1$ meV near the $\overline{M}$ point. Uncertainties in the zero of binding energy arising from drifts in photon energy or power supplies lead to an additional uncertainty of ± 0.5 meV. This consideration applies to all the data, not just at $\overline{M}$.

Next, consider the spectrum along the ΓY (π, π) direction (labeled 12). Again, the shape of the leading edge is dominated by the energy resolution at 13 K (but not in the normal state, where the Fermi function dominates). Unlike the $\overline{M}$ point, the momentum resolution affects the result along the (π, π) direction and nearby points, where the band is rapidly dispersing; the momentum window leads to an effective broadening of the EDC via $\delta\omega_\mathbf{k} = \mathbf{v}_F \delta\mathbf{k}$ ($\mathbf{v}_F$ is the Fermi velocity). This affects the high binding energy side leading to a rather broad feature in the EDC even at 13 K. In calculations this effect is incorporated through $\varepsilon_\mathbf{k}$, for which we use the same tight-binding fit to the normal-state ARPES described above. Using the same Γ as before, again the fit is obtained by only varying $\Delta_\mathbf{k}$ and I_0. Since the broad EDC consists of many sharp unresolved peaks, it is only the leading edge of the EDC which is sensitive to the gap. We find $|\Delta_\mathbf{k}| = 3 \pm 2.5$ meV. The inset in this diagram shows the best fit (solid line), together with fits for $|\Delta_\mathbf{k}| = 1$ and 5 meV (dotted lines), which enclose all the experimental points. Applying the same considerations, we find $|\Delta_\mathbf{k}| = 7 \pm 2.5$ meV along ΓX (labeled 3). A zero gap curve is shown for comparison.

Finally, consider the point labeled 14, where the same considerations as those in the case of the (π, π) direction apply. The best fit is obtained with a zero gap. Note that we would not be able to obtain a nonzero value by changing any of the parameters [14] in our fits where a zero gap is observed.

The final results of the fits are shown in Fig. 4. We measured several samples, and the results are reproducible [15]. Even though these results were obtained by fitting, we note that we obtain a similar structure in $|\Delta_\mathbf{k}|$ if we plot the binding energy of the midpoint of the leading edge of the spectra, although the absolute values are smaller. The most striking feature in Fig. 4 is that the gap is highly anisotropic, being large in the vicinity of the $\overline{M}$ point and small along the ΓX and ΓY directions, consistent with the original results of Shen *et al.* [4]. However, $|\Delta_\mathbf{k}|$ is *not* zero along these (π, π) directions, as previously noted by Kelley *et al.* [5]. Rather, it becomes zero on both sides. The two-node feature is reproducible in our measurements, being observed in different samples with different orientations. The cusps at the node points may indicate a change in sign of the gap functions. We note that Fig. 4 implies that the gap function has an

extremum along the ΓX and ΓY directions, which cannot be understood in the $d_{x^2-y^2}$ scenario even if a small component of another symmetry were admixed, which would simply move the node to one side of the (π, π) lines, but would not have nodes on both sides. Of course, in the anisotropic s-wave scenario, there is no symmetry restriction on the nodes. For instance, an extended s-wave gap in general has two nodes per quadrant, consistent with our data.

Therefore, if we ignore the superlattice, we come to the conclusion that our data are consistent with the anisotropic s-wave scenario. The superlattice, however, complicates this simple interpretation in the ΓX quadrant. It introduces the umklapp FS sheets shown in Fig. 1. Note that the nodes in the gap in this quadrant occur where normal and umklapp bands cross. One can show [16] that, for a d-wave state, a node in the gap will occur at these crossing points if the superlattice potential is larger than the order parameter, a rather weak condition. This is a phase-sensitive argument peculiar to a gap function which changes sign about the (π, π) directions. This argument would not apply in the ΓY quadrant, and, since similar behavior is being seen in this quadrant, a d-wave state does not appear to be consistent with our data at the present time.

In conclusion, we find a nontrivial dependence of the superconducting gap in $Bi_2Sr_2CaCu_2O_8$, with line nodes on both sides of the (π, π) directions, consistent with an anisotropic s-wave gap [17].

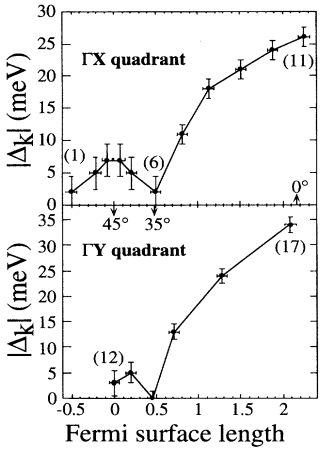

FIG. 4. Absolute values of the superconducting gap along the FS in Bi2212. The numbers on the points correspond to the data labeled in Fig. 2. The x axis is in units of k (the length of Γ-$\bar{M}$ is π). Some angles relative to the X, Y-$\bar{M}$ direction are also indicated.

This work is supported by the DOE under Contract No. W-31-109-ENG-38 and by NSF Grant No. 8914120. The Synchrotron Radiation Center is supported by NSF Grant No. DMR-9212658.

[1] B. G. Levi, Phys. Today **46**, No. 5, 17 (1993).
[2] W. N. Hardy *et al.*, Phys. Rev. Lett. **70**, 3999 (1993).
[3] C. G. Olson *et al.*, Science **245**, 731 (1989).
[4] Z.-X. Shen *et al.*, Phys. Rev. Lett. **70**, 1553 (1993).
[5] R. J. Kelley *et al.*, Phys. Rev. B **50**, 590 (1994).
[6] The detailed measurements of the Fermi surface will be presented in a future publication.
[7] A six parameter fit was used, as in the work of R. J. Radtke and M. R. Norman [Phys. Rev. B **50**, 9554 (1994)], although with parameters to fit our data.
[8] R. L. Withers *et al.*, J. Phys. C **21**, 6067 (1988). We also see the superlattice with x-ray diffraction in our own samples.
[9] P. Aebi *et al.*, Phys. Rev. Lett. **72**, 2757 (1994). Recently, these authors [J. Osterwalder *et al.* (to be published)] have also reported superlattice features.
[10] While the Bi2212 EDC is a spectral function, the polycrystalline nature of Pt leads to an angle integrated EDC which measures density of states. Note, however, that at 13 K the shapes of the leading edges of both the Bi2212 and Pt spectra are determined by the energy resolution.
[11] J. R. Schrieffer, *Theory of Superconductivity* (W. A. Benjamin, New York, 1964), p. 122.
[12] We use a background of the form $c \int_{\omega}^{+\infty} d\varepsilon\, I(\mathbf{k}, \varepsilon)$, which is a phenomenological model of secondary emission of inelastically scattered electrons, with the same value of c for all spectra.
[13] Similar behavior is observed in optical and microwave measurements of $YBa_2Cu_3O_{6.95}$ [D. A. Bonn *et al.*, Phys. Rev. Lett. **68**, 2390 (1992)].
[14] In particular, we cannot get a finite $|\Delta_{\mathbf{k}}|$ even after setting $\varepsilon_{\mathbf{k}} \neq 0$, since the leading edge of the spectrum would shift to the high binding energy side, which is inconsistent with the data.
[15] The data shown in the two quadrants were taken on different samples (from the same batch) because our analyzer does not have the angular range to cover both quadrants in the geometry used.
[16] M. R. Norman, M. Randeria, H. Ding, and J. C. Campuzano (to be published).
[17] We find that a gap of the form $\cos k_x \times \cos k_y$ fits the data quite well including the position of the nodes [16].